Materials Transactions, Vol. 55, No. 10 (2014) pp. 1599 to 1605

EXPRESS REGULAR ARTICLE

Two-Dimensional Observation of Grain Boundary Sliding of ODS Ferritic Steel in High Temperature Tension

Hiroshi Masuda[1,*1], Satoshi Taniguchi[1,*2], Eiichi Sato[1], Yoshito Sugino[2,*3] and Shigeharu Ukai[2]

[1]*Institute of Space and Astronautical Science, Japan Aerospace Exploration Agency, Sagamihara 252-5210, Japan*
[2]*Materials Science and Engineering, Faculty of Engineering, Hokkaido University, Sapporo 060-8628, Japan*

High-temperature tensile deformation was performed using ODS ferritic steel, which has grain structure largely elongated and aligned in one direction, in the direction perpendicular to the grain axis. In the superplastic region II, two-dimensional grain boundary sliding (GBS) was achieved, in which the material did not shrink in the grain-axis direction and grain-boundary steps appeared only in the surface perpendicular to the grain axis. In this condition, a classical grain switching event was observed. Using kernel average misorientation maps drawn with SEM/EBSD, dominant deformation mechanisms and accommodation processes for GBS were examined in the different regions. Cooperative grain boundary sliding, in which only some of grain boundaries slide, was also observed. [doi:10.2320/matertrans.M2014115]

(Received April 1, 2014; Accepted July 11, 2014; Published August 29, 2014)

Keywords: *superplastic deformation, grain boundary sliding, grain switching, microgrid*

1. Introduction

Superplasticity, first found by Pearson in 1934,[1)] is a high-temperature deformation mode of polycrystalline materials. This phenomenon, which occurs in particular alloys and ceramics of fine grain structure, shows extremely large elongation over hundreds of percent in tension without localized necking. Superplasticity is useful for near-net-shape forming of thin and complicated components for aerospace industries. At Institute of Space and Astronautical Science (ISAS/JAXA), titanium-alloy fuel and gas tanks for the reaction control system of spacecrafts have been fabricated using superplasticity.[2)]

Grain boundary sliding (GBS) and its accommodation are operating as dominant mechanisms for superplastic deformation. However, fundamental details of GBS and its accommodation have not been revealed completely yet. To date, grain movement and rearrangement with superplastic deformation have been confirmed through observing the material surface after deformation.[1,3–5)] Initially-flat surfaces show steps at grain boundaries because of out-of-plane GBS.[1)] In addition, surface markers such as scratches have shown offsets at grain boundaries because of in-plane GBS.[3)] Recently, instead of scratches, fine regular grids drawn by a focused ion beam (FIB) have been used, which has facilitated detailed analyses.[4,5)]

However, these surface studies mainly entail two problems that make this issue complex. First, deformation modes can be different between those at surfaces and inside of materials because grains at surfaces are less restricted by other grains around than those inside, which may make surface grains move more easily. Next, in tensile deformation, materials have negative strains perpendicular to the tensile direction to conserve their volume. Therefore, emergence of new grains onto the surface during deformation has been observed, which makes observation difficult.

To address the first problem, Matsuki *et al.* introduced internal line markers and observed offsets of the lines.[6)] Although it constitutes strong evidence of GBS inside the material, this internal marker was merely a line of oxide particles introduced by diffusion bonding of two plates of aluminum alloy. Therefore it is unable to bring about a precise analysis. To resolve the second problem, Rust and Todd tried to restrict deformation two-dimensionally using shear deformation.[7)] Although they obtained macroscopically-two-dimensional superplastic deformation, microscopic surface-grain movement was still not restricted to the in-plane direction. Therefore they also left the first problem unsolved.

In this study, we aimed to solve these problems by surface observation of two-dimensional GBS in oxide-dispersion-strengthened (ODS) ferritic steel. This material has been developed for the next-generation fuel-cladding tubes of sodium-cooled fast breeder reactors.[8)] This steel has characteristic grain structure that is largely elongated in one direction. It shows depression of strength in high-temperature tension perpendicular to the grain axis, which intimates the presence of GBS.[9,10)] When this steel deforms in tension perpendicular to the grain axis at an optimum condition for GBS, only two-dimensional grain movement is expected to operate as if a bundle of pencils was stretched. In addition, the surface observation is expected to represent the bulk deformation because the grains are sufficiently elongated from the surface to its inside that they are not much influenced by the surface conditions.

2. Experimental Procedure

The ODS ferritic steel we used for this study has the following chemical compositions: 15Cr-0.03C-2W-3.8Al-0.32Zr-0.12Ti-0.35Y_2O_3 (mass%). This steel shows single α phase in the all temperature range.[9)] It was mechanically alloyed from ferrite and yttria powder, heat-treated at 1423 K,

*[1]Graduate Student, The University of Tokyo. Corresponding author, E-mail: masuda.hiroshi@ac.jaxa.jp
*[2]Graduate Student, The University of Tokyo. Present address: Oita Works, Nippon Steel and Sumitomo Metal Corporation, Ltd., Oita 870-0992, Japan
*[3]Graduate Student, Hokkaido University

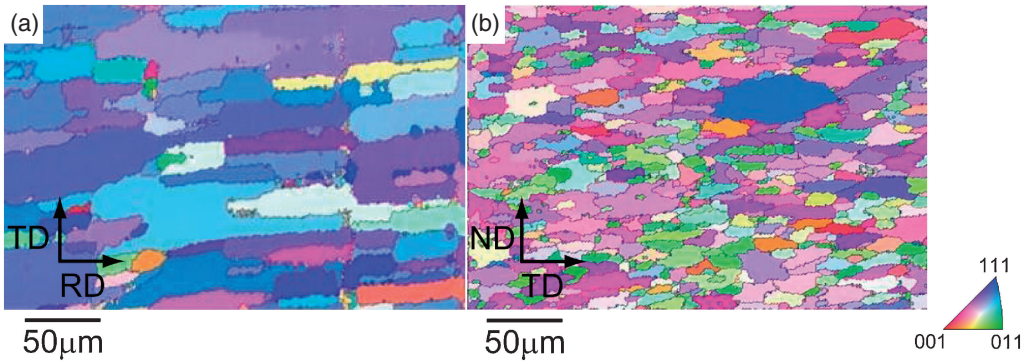

Fig. 1 Inverse Pole Figure (IPF) maps of ODS ferritic steel recrystallized at 1423 K: (a) in the ND plane, and (b) in the RD plane.

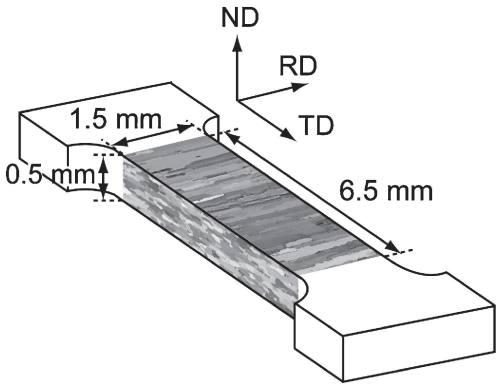

Fig. 2 Schematic of a tensile test specimen. The tensile direction is perpendicular to the grain axis.

cold-rolled to a reduction of 85%, annealed at 1423 K for 4 h, and water-quenched. Figure 1 shows the recrystallized microstructure observed with an electron back-scattered diffraction pattern (EBSD) method on a scanning electron microscope with a field emission gun (FE-SEM). The grain sizes measured using the linear intercept method were 120 μm in the rolling direction (RD), 11 μm in the normal direction (ND) and 21 μm in the transverse direction (TD). The grain structure largely elongated in RD is caused by the heavy rolling and strong pinning against grain boundary migration by yttria particles.[11)]

Tensile specimens were cut with an electric discharge machine with the tensile direction parallel to TD, to have a gauge length of 6.5 mm, width of 1.5 mm in RD and thickness of 0.5 mm in ND (Fig. 2). The side surfaces of the gauge section (RD surfaces) were mechanically polished. Then they were electro-polished in a solution of 90% acetic acid and 10% perchloric acid at 15 V for 30 s at room temperature. After microstructural observation with an SEM/EBSD with its step sizes of 0.2 μm, a 20 × 20 grid consisting of 0.3-μm-width lines with 5-μm intervals was drawn using an FIB.

Tensile tests and a creep test were conducted at 1173 K in vacuum of about 10^{-4} Pa in a hydraulic servo fatigue testing machine coupled with a high-frequency induction heating facility. The engineering tensile strain rates were, respectively, 1.0×10^{-3}, 1.0×10^{-4}, 1.0×10^{-5} and $3.8 \times 10^{-6}\,s^{-1}$. For a lower strain rate, a creep test was conducted with stress of 27 MPa. All the tests were continued until fracture.

After deformations, the RD-surface grids and the RD- and ND-surface profiles were observed using a laser microscope. For SEM/EBSD observation of the RD surface after deformations, we needed slight ion-polishing of about 100 nm with a cross-section polisher. It must be noted that the polishing depth was much shallower than that of about 4 μm by mechanical polishing in our latest paper.[12)] The orientation image map observed after deformations were compared with those before deformations. It was confirmed that grain structure was maintained and that significant recrystallization did not occur during deformation at 1173 K. Kernel average misorientation (KAM) maps were drawn for estimating local crystal misorientations and the dislocation structure.

3. Results

3.1 Mechanical behavior

Figure 3(a) shows the engineering stress–strain curves of the tensile tests, and Fig. 3(b) shows the creep curve, which can be regarded as a tensile test at the steady-state-creep rate; $9.2 \times 10^{-8}\,s^{-1}$. The relation between the flow stress σ and the strain rates $\dot{\varepsilon}$ is shown logarithmically in Fig. 4. This sigmoidal curve is divided into three regions, which are conventionally called regions I, II and III, respectively, with low, high, and again low values of the strain rate sensitivity index m given as

$$m = \partial \ln \sigma / \partial \ln \dot{\varepsilon}. \quad (1)$$

It has been experimentally demonstrated that a material shows superplastic behavior when m value gets over 0.3 in region II.[13,14)] In this case, the m value reached 0.35 at $1.0 \times 10^{-5}\,s^{-1}$. In spite of the high m value, however, the elongation at this strain rate was only about 8%, which is discussed later.

3.2 Two-dimensionality of deformation

Figure 5 shows the reductions of the specimens' width (RD) and thickness (ND) at 1% tensile strain. They were calculated from the reduction and the elongation at fracture. In the deformations at the strain rates higher than $1.0 \times 10^{-4}\,s^{-1}$, i.e., in region III, both reductions had the close values of about 0.4%, about a half of the tensile strain, which means that the deformations were isotropic in the directions perpendicular to the tensile axis. However, in the deforma-

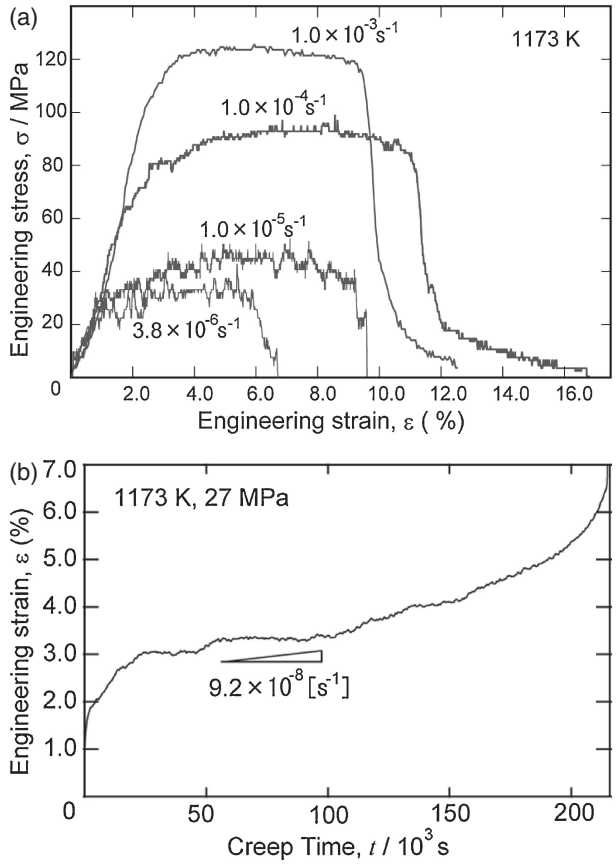

Fig. 3 (a) Engineering stress–strain curves of four tensile tests. (b) Creep curve with a stress of 27 MPa and the strain rate is estimated to be $9.2 \times 10^{-8}\,s^{-1}$ from the average rate between 40 and 120×10^3 s.

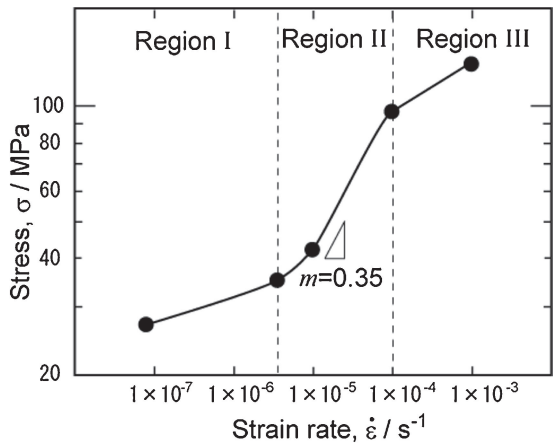

Fig. 4 Logarithm plots of the stress and the strain rate. At $1.0 \times 10^{-5}\,s^{-1}$, the strain rate sensitivity index m reached the maximum value of 0.35.

tions at strain rates below $1.0 \times 10^{-5}\,s^{-1}$, i.e., in region II, the thickness reduction was large about 0.7%, while the width reduction was small about 0.1%, which means that the material shrank only in ND with almost the amount of the tensile elongation. That fact indicates that the deformation occurred two-dimensionally and that it was restricted in the direction parallel to the grain axis in region II.

3.3 Surface conditions after deformation

Figures 6 and 7 respectively portray profiles of the initially-polished RD and ND surfaces observed using a

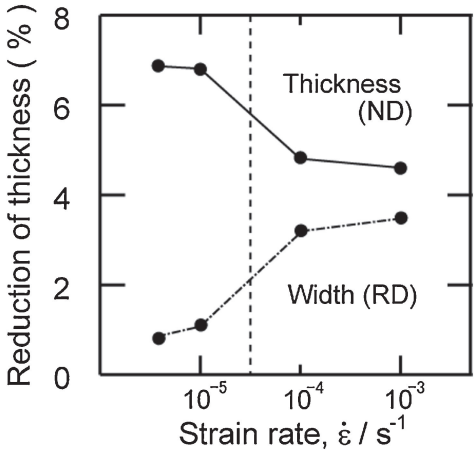

Fig. 5 Reductions of thickness (ND) and width (RD) between before and after deformations at different strain rates normalized to a strain of 10%.

laser microscope after deformations at $1.0 \times 10^{-5}\,s^{-1}$ in region II and $1.0 \times 10^{-3}\,s^{-1}$ in region III. As mentioned in the Sec. 2., the oxide layer which resulted from high-temperature deformation was thin enough that 100-nm-ion-polishing could remove it.

At $1.0 \times 10^{-5}\,s^{-1}$, although both surfaces show steps at grain boundaries, the step heights are less than 0.5 μm on the RD surface whereas some are more than 3 μm in the ND surface. That fact indicates that GBS occurred two-dimensionally and that it was restricted within the RD surface. It just seems that a bundle of pencils was stretched.

On the contrary, at $1.0 \times 10^{-3}\,s^{-1}$, such large steps were not observed, which indicates that GBS did not occur in region III.

3.4 GBS and grain switching event

Figures 8 show microgrids before and after deformations of 7–10% at different strain rates observed by an SEM or a laser microscope. Details are discussed later with KAM-map observation.

Figures 9(a) and 9(b) show the inverse pole figure (IPF) maps of the same area of Fig. 8(d), before and after the deformation at $1.0 \times 10^{-5}\,s^{-1}$, respectively. Figures 10(a) and 10(b) show the magnified views of the areas represented as bold squares in Figs. 9(a) and 9(b), respectively. The same grains can be traced before and after the deformation in Figs. 10. Before the deformation, grains A and B were touching each other and other grains C and D were separated by A and B. After the deformation, grains C and D became touching each other while grains A and B became separated. This clear example of a grain switching event, which resulted from GBS, can be regarded as a potent fundamental process producing a large elongation in superplastic deformation.[15] It is astonishing that a switching event was observed in a small strain of 8%; the classical Ashby and Verrall model tells that one switching event generate a strain of 55%.[15]

3.5 KAM map by SEM/EBSD

Figure 11 shows KAM maps observed by SEM/EBSD after deformations at different strain rates. It is expected that there exist high-density geometrical necessary dislocations where the KAM contrast is strong.[16] This analysis indicates

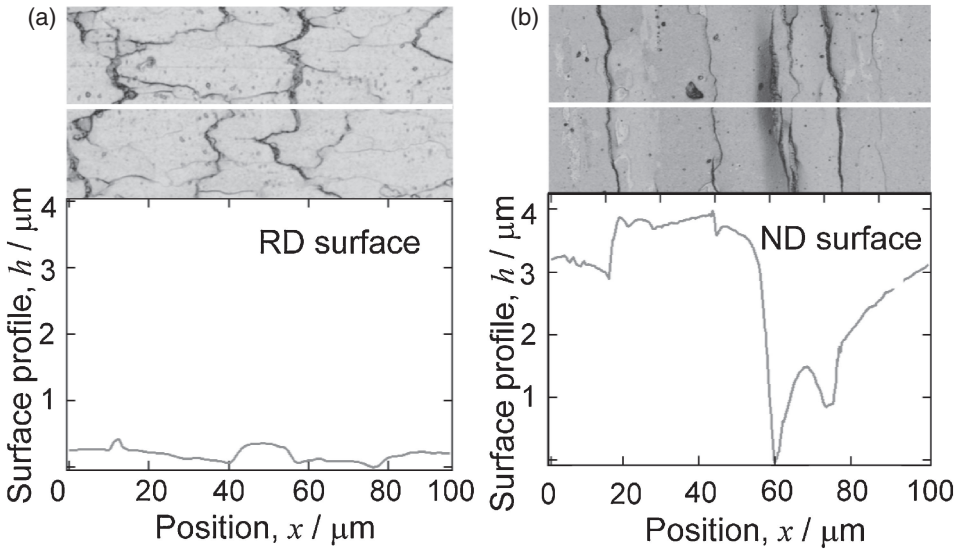

Fig. 6 Surface profiles measured using a laser microscope after deformation at $1.0 \times 10^{-5}\,s^{-1}$ in (a) the RD surface and (b) the ND surface.

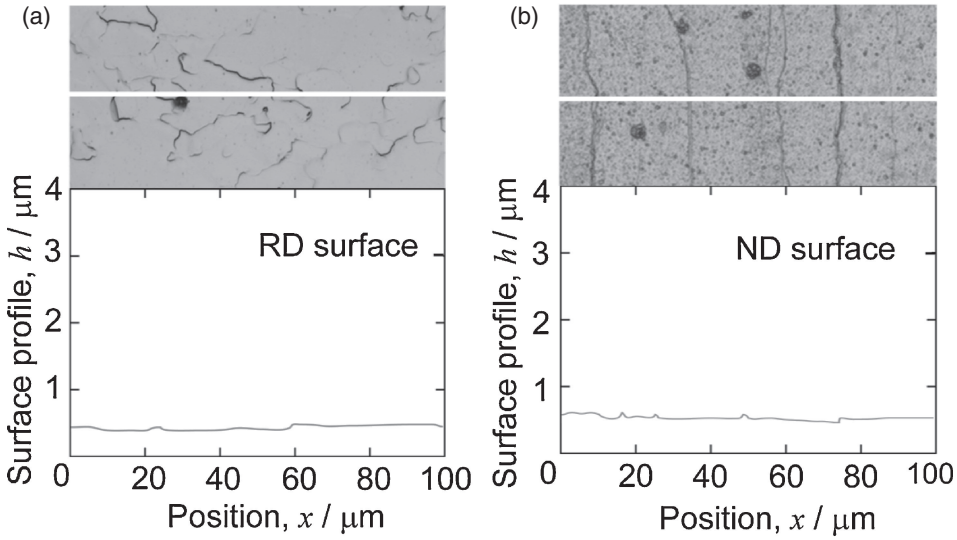

Fig. 7 Surface profiles measured using a laser microscope after deformation at $1.0 \times 10^{-3}\,s^{-1}$ in (a) the RD surface and (b) the ND surface.

the dominant mechanism of deformation and the accommodation for GBS at each strain rate, as follows: (i) At $1.0 \times 10^{-3}\,s^{-1}$ in region III, no gaps in the grid are observed (Fig. 8(b)) and the KAM contrast spreads throughout the view (Fig. 11(a)). It indicates that the deformation was dominated by dislocation movement, whereas GBS did not occur. (ii) At $1.0 \times 10^{-4}\,s^{-1}$ in the transition between regions III and II, some gaps in the grid are seen at white circles in Fig. 8(c), and the KAM contrast is strong around some of the grain boundaries (Fig. 11(b)). It is understood that GBS occurred at some of the grain boundaries during the deformation, accommodated by dislocations, which were finally stacked around grain boundaries; they are traced by red lines in Fig. 11(c). (iii) Also at $1.0 \times 10^{-5}\,s^{-1}$ in region II, some gaps are visible in the grid (Fig. 8(d)), but the KAM contrast in Fig. 11(d) is weaker than that shown in Fig. 11(b); grain boundaries which slid are traced by red lines in Fig. 11(e). Therefore, it is implied that the deformation was dominated by GBS, which was accommodated at the grain boundaries by some mechanism without local misorientations.

4. Discussion

4.1 Macroscopic and microscopic behavior in region II

The optimum strain rate for region II deformation of this material at 1173 K is found to be $1.0 \times 10^{-5}\,s^{-1}$ from the maximum value of the strain rate sensitivity m. Nevertheless, the tensile strain at this rate was only 8%, which is much less than a superplastic elongation.

It is necessary for continuous superplastic deformation that grains can move avoiding stress concentration; the largest stress concentration is generated at grain triple points in two-dimensional grain structure, while it is generated at 4-fold points in three-dimensional one. It must be noted that almost all of superplastic theories estimating the amount of

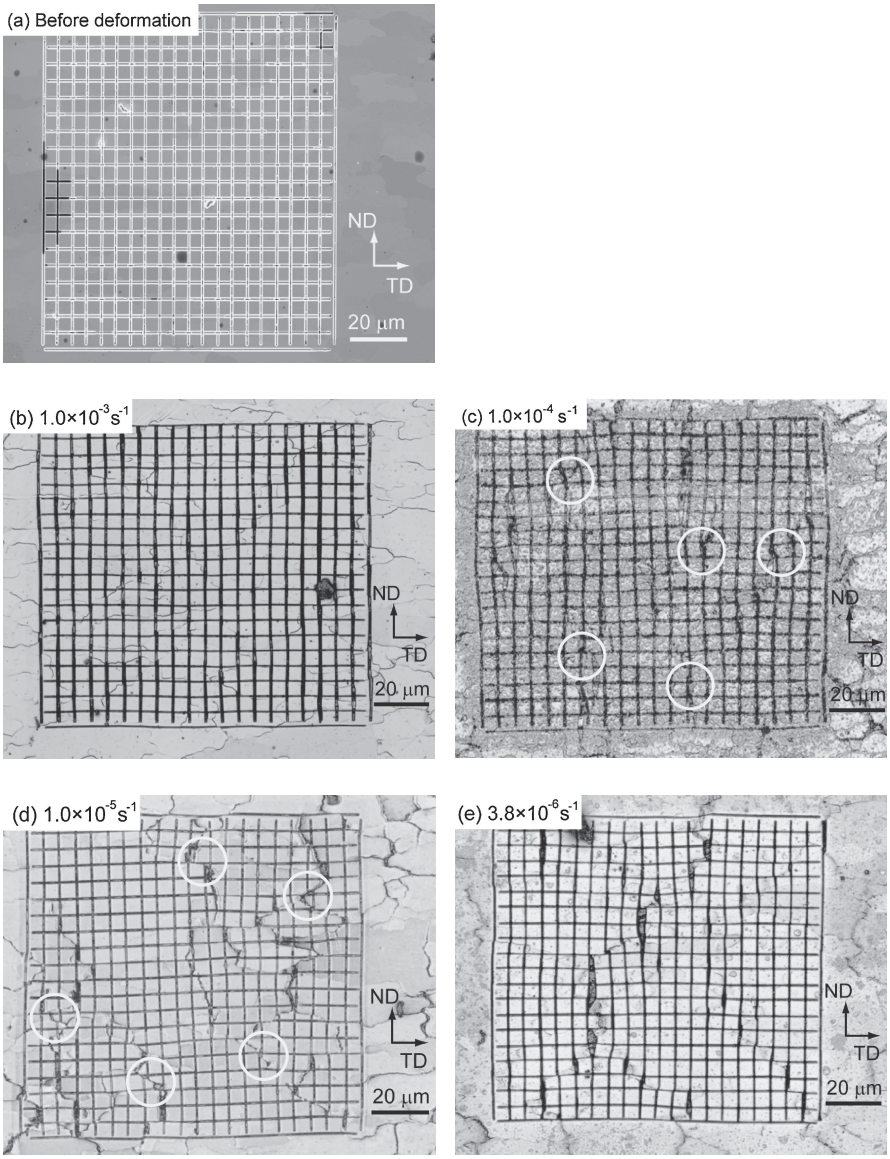

Fig. 8 Microgrid milled on the RD surface by an FIB and observed (a) before deformation with an SEM, and (b) after deformations at $1.0 \times 10^{-3}\,s^{-1}$, (c) at $1.0 \times 10^{-4}\,s^{-1}$, (d) at $1.0 \times 10^{-5}\,s^{-1}$, and (e) at $3.8 \times 10^{-6}\,s^{-1}$ with a laser microscope. In (c) and (d), some of grid gaps are pointed by white circles.

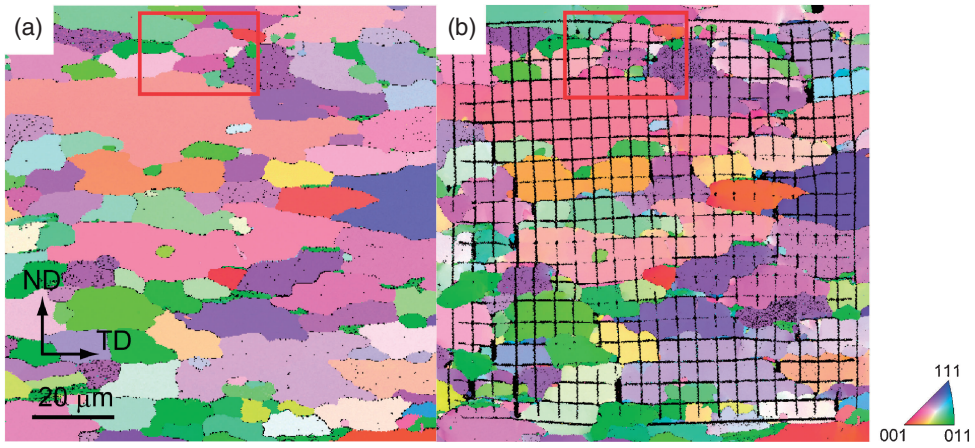

Fig. 9 IPF maps of the same view in the RD surface before and after deformation at $1.0 \times 10^{-5}\,s^{-1}$ with Fig. 8 (a) and (d) respectively.

accommodation have been based on the two-dimensional grain structure, including the classical grain switching model.[15] In the three-dimensional case, however, it is easy to imagine that each grain can find an easier way of moving with less amount of accommodation perpendicular to the two-dimensional plane than within the plane. It is, therefore,

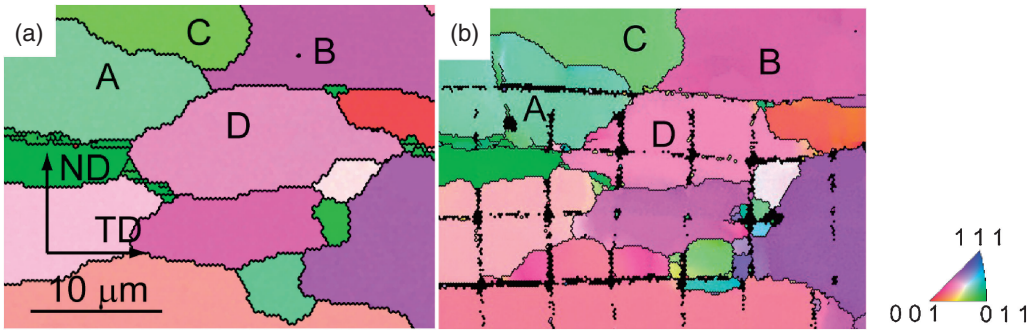

Fig. 10 Magnified views of the marked squares of Figs. 9(a) and 9(b), respectively. Grain A touched B before deformation, whereas grain C touched D after deformation, which shows a grain neighbor switching event as a result from GBS.

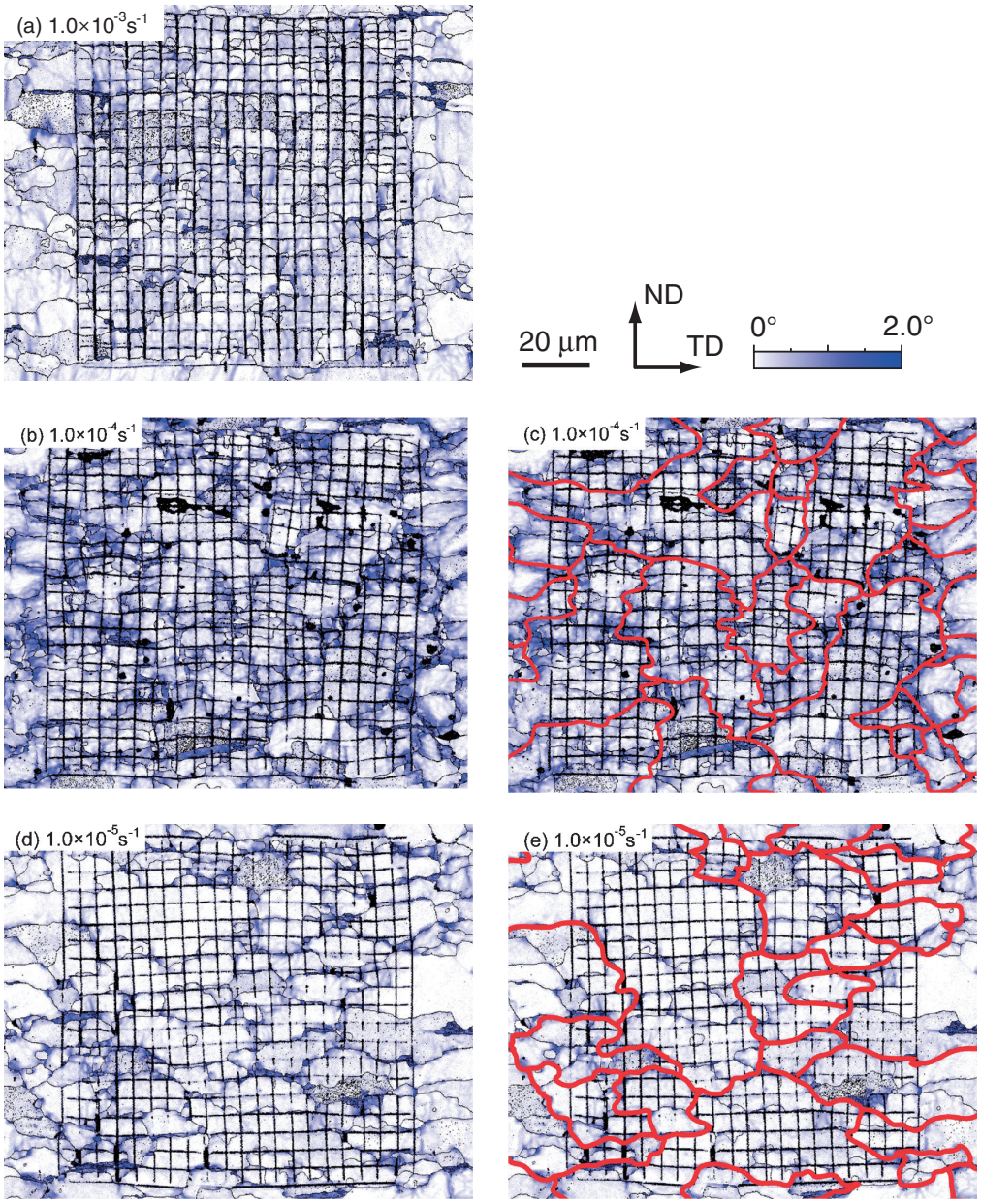

Fig. 11 KAM map in the RD plane after deformation at each strain rate. Intensity of the contrast shows the geometrical necessary dislocation density. Red lines in the figures show grain boundaries which slid. They are clarified by grid observation and located on grain boundaries with strong KAM contrasts. (a) $1.0 \times 10^{-3}\,s^{-1}$, in region III, (b)(c) $1.0 \times 10^{-4}\,s^{-1}$, in transitions region between III and II, and (d)(e) $1.0 \times 10^{-5}\,s^{-1}$, in region II.

considered that in the present case of two-dimensional GBS, the accommodation, which is much less sufficient than in the case of three-dimensional one, led the early fracture.

Detailed observation of the accommodation process at grain triple points in ODS ferritic steel is now under way, which will contribute to experimental verification

and construction of two-dimensional modeling of superplasticity.

4.2 Deformation mechanism in each region

From KAM maps in Figs. 11, the dominant deformation mechanisms and its accommodation with GBS can be discussed.

In region III, at $1.0 \times 10^{-3}\,s^{-1}$, the deformation was dominated by dislocation movement inside of individual grains without GBS. In the KAM map (Fig. 11(a)), some strong contrast is crossing grains, which represent subgrain boundaries developed during dislocation creep. This fact corresponds to the result that no gap is observed in the grid (Fig. 8(b)).

In the transition between regions III and II, at $1.0 \times 10^{-4}\,s^{-1}$, GBS occurs and is accommodated by the movement of dislocations at grain boundaries, which are stacked at boundaries and creates strong KAM contrast. In addition, subgrain boundaries are observed across some grains, which indicate the operation of the dislocation creep mechanism. In this region, the dominant mechanism is transferring from dislocation creep to GBS. Therefore, GBS is accommodated by dislocation creep, which relieves the stress concentration.

It should also be described that GBS does not occur and that KAM contrast is hardly observed at some grain boundaries in this transition region. They mainly correspond to those nearly parallel or perpendicular to the tensile direction which are difficult to be sheared. Such groups of grains moved cooperatively having little misorientation among neighbors. This phenomenon, called cooperative grain boundary sliding (CGBS), has been regarded as an important mechanism for superplastic deformation.[17] Although this phenomenon is difficult to observe in Fig. 8(c), it is more easily observed on the KAM map in Figs. 11(b) and 11(d), i.e. the groups of the grains are surrounded with the KAM contrasts and together with red lines indicating where CGBS occurred, respectively (Figs. 11(c) and 11(e)).

In region II, at $1.0 \times 10^{-5}\,s^{-1}$, deformation was dominated by GBS accommodated by some mechanism without local misorientation, which is expected to be mass transport by diffusion process. This result corresponds to previous works that could not observe intragranular slips in region-II superplastic deformation.[1,4,5,7] Furthermore, in this region, occurrence of CGBS can be confirmed. It is a fundamental mechanism also in this region, too. It is desired to obtain stronger evidence of mass transport near grain boundaries through finer grid observation in future works.

About in region I, we have not gotten a potent result to explain the mechanism because of surface damage of the sample during the deformation. It shall be investigated in future works.

5. Conclusion

This study made direct observation of GBS restricted two-dimensionally using ODS ferritic steel with crystal grain structure largely elongated and aligned in one direction. Deformation mechanisms were examined using surface microgrids milled by FIB and KAM maps observed using SEM/EBSD. We obtained the following conclusions:

(1) In tensile tests perpendicular to the grain axis, the deformation was isotropic in directions perpendicular to the tensile axis at high strain rates although it was two-dimensional and restricted to the RD plane at appropriate strain rates.
(2) In region III, deformation was dominated by dislocation motions without GBS.
(3) In the transition between region III and II, CGBS occurred. It was accommodated by dislocation movement around grain boundaries which slid.
(4) In region II, deformation was dominated by CGBS with few dislocation activities. It was accommodated by some mechanism without local misorientation in crystals, which can be a diffusional process.
(5) Also in this region, the classical two-dimensional grain switching event was observed.

Acknowledgments

The use of FIB in this work was supported by Nanotechnology Platform (project No. 12024046) of MEXT, Japan.

REFERENCES

1) C. E. Pearson: J. Inst. Metals **54** (1934) 111–124.
2) E. Sato, S. Sawai, K. Uesugi, T. Takami, K. Furukawa, M. Kamada and M. Kondo: Mater. Sci. Forum **551–552** (2007) 43–48.
3) K. Matsuki, Y. Ueno and M. Yamada: J. Japan Inst. Metals **38** (1974) 1136–1144.
4) M. A. Rust and R. I. Todd: Mater. Sci. Forum **551–552** (2007) 615–620.
5) K. Sotoudeh and P. S. Bate: Acta Mater. **58** (2010) 1909–1920.
6) K. Matsuki, H. Morita, M. Yamada and Y. Murakami: Met. Sci. **11** (1977) 156–163.
7) M. A. Rust and R. I. Todd: Acta Mater. **59** (2011) 5159–5170.
8) S. Ukai, M. Harada, H. Okada, M. Inoue, S. Nomura, S. Shikakura, K. Asabe, T. Nishida and M. Fujiwara: J. Nucl. Mater. **204** (1993) 65–73.
9) S. Ukai, T. Okuda, M. Fujiwara, T. Kobayashi, S. Mizuta and H. Nakashima: J. Nucl. Sci. Technol. **39** (2002) 872–879.
10) Y. Sugino, S. Ukai, B. Leng, Q. Tang, S. Hayashi, T. Kaito and S. Ohtsuka: ISIJ Int. **51** (2011) 982–986.
11) H. Sakasegawa, S. Ohtsuka, S. Ukai, H. Tanigawa, M. Fujiwara, F. Ogiwara and A. Kohyama: Fusion Eng. Des. **81** (2006) 1013–1018.
12) S. Taniguchi, N. Kawai and E. Sato: Mater. Sci. Forum **735** (2012) 79–83.
13) W. A. Backofen, I. R. Truner and D. H. Avery: Am. Soc. Met. **57** (1964) 980–990.
14) D. L. Holt and W. A. Backofen: Trans. Am. Soc. Met. **59** (1966) 755–768.
15) M. F. Ashby and R. A. Verrall: Acta Metall. **21** (1973) 149–163.
16) M. Kamaya: Ultramicroscopy **111** (2011) 1189–1199.
17) R. Raj and M. F. Ashby: Metall. Trans. **2** (1971) 1113–1127.